Title

Hydrodynamic pressures on rigid walls subjected to cyclic and seismic ground motions

Journal

Earthquake Engineering & Structural Dynamics, 53(1)

ISSN

0098-8847

Authors

AlKhatib, Karim

Hashash, Youssef MA

Ziotopoulou, Katerina

et al.

Publication Date

2024

DOI

10.1002/eqe.4020

Peer reviewed

Received: 25 April 2023 | Revised: 11 September 2023 | Accepted: 14 September 2023

DOI: 10.1002/eqe.4020

RESEARCH ARTICLE

WILEY

Hydrodynamic pressures on rigid walls subjected to cyclic and seismic ground motions

Karim AlKhatib[1] | **Youssef M. A. Hashash**[1] | **Katerina Ziotopoulou**[2] | **Brian Morales**[3]

[1]Department of Civil and Environmental Engineering, University of Illinois Urbana-Champaign, Urbana, Illinois, USA

[2]Department of Civil and Environmental Engineering, University of California, Davis, California, USA

[3]Fugro USA Land, Inc., Walnut Creek, California, USA

Correspondence
Youssef M. A. Hashash, Department of Civil and Environmental Engineering, University of Illinois Urbana-Champaign, Urbana, IL 61801, USA.
Email: hashash@illinois.edu

Funding information
National Science Foundation, Grant/Award Numbers: CMMI-1762749, CMMI-1763129

Abstract

Seismic design of water retaining structures relies heavily on the response of the retained water to shaking. The water dynamic response has been evaluated by means of analytical, numerical, and experimental approaches. In practice, it is common to use simplified code-based methods to evaluate the added demands imposed by water sloshing. Yet, such methods were developed with an inherent set of assumptions that might limit their application. Alternatively, numerical modeling methods offer a more accurate way of quantifying the water response and have been commonly validated using 1 g shake table experiments. In this study, a unique series of five centrifuge tests was conducted with the goal of investigating the hydrodynamic behavior of water by varying its height and length. Moreover, sine wave and earthquake motions were applied to examine the water response at different types and levels of excitation. Arbitrary Lagrangian-Eulerian finite element models were then developed to reproduce 1 g shake table experiments available in the literature in addition to the centrifuge tests conducted in this study. The results of the numerical simulations as well as the simplified and analytical methods were compared to the experimental measurements, in terms of free surface elevation and hydrodynamic pressures, to evaluate their applicability and limitations. The comparison showed that the numerical models were able to reasonably capture the water response of all configurations both under earthquake and sine wave motions. The analytical solutions performed well except for cases with resonance under harmonic motions. As for the simplified methods, they provided acceptable results for the peak responses under earthquake motions. However, under sine wave motions, where convective sloshing is significant, they underpredict the response. Also, beyond peak ground accelerations of 0.5 g., a mild nonlinear increase in peak dynamic pressures was measured which deviates from assumed linear response in the simplified methods. The study confirmed the reliability of numerical models in

capturing water dynamic responses, demonstrating their broad applicability for use in complex problems of fluid-structure-soil interaction.

KEYWORDS
arbitrary Lagrangian-Eulerian, centrifuge, hydrodynamics, retaining structures, water sloshing

1 | INTRODUCTION

Water retaining structures are required to exhibit seismic resilience during earthquakes due to their important role in supplying potable and emergency water and the potential damage that can be caused by the sudden release of the stored water. However, the code-based and simplified methods commonly used for their design are not always applicable, which raises concerns regarding the reliability and performance of these structures. In order to properly study their resilience to earthquake damage, one needs to cumulatively consider the interactions between the surrounding soil, the structure itself, and the enclosed water during an earthquake. To this date, the latter component has been the least studied.

Liquid sloshing is a complex free surface flow that increases the hydrodynamic demands on retaining structures during shaking. Since the early 1960s, the phenomenon of liquid sloshing has been the main subject of studies in aerospace engineering due to the motion of liquids inside the tanks of aerospace vehicles,[1] in maritime applications where the movement of liquids on board was found to induce ship instabilities,[2,3] and then emerged into other fields including water retaining structures. At the time, the understanding of the fluid dynamic response inside containers was mainly derived from closed-form analytical solutions. Graham and Rodriguez[4] provided analytical solutions for the natural frequency, pressure distribution, and water height change inside rectangular tanks subjected to horizontal shaking. Their solution assumes an incompressible and non-viscous fluid with small free surface displacements and is only applicable for harmonic (sinusoidal) motions with frequency content far from the natural frequency of the water body to avoid resonance. Graham and Rodriguez[4] also proposed an idealized equivalent mass-spring mechanical system. Dodge[5] referenced work from Abramson[6] that solved the water response under resonance and non-resonance conditions by introducing damping factors into the equations that can be determined experimentally. In the field of civil engineering, simplified design procedures were developed to approximate the hydrodynamic pressure demands on structure.[7,8] Most of these procedures, commonly used in practice and research as well as design standards,[9,10,11] assume linear scaling with peak ground motion intensities.

Numerous small scale 1 g shake table experiments can be found in the literature,[12–18] which specifically investigate water hydrodynamics and validate related numerical models. Nevertheless, little experimental research that studies water hydrodynamics under a scaled (centrifuge) environment is available. Such work is needed to evaluate the effects of scaling on the dynamic behavior of water and explore its agreement with the scaling laws. Furthermore, and given the reduced scale, such experiments would be more cost- and time-efficient in exploring more than one configuration at a time.

Numerical modeling is now a common and reliable approach for studying liquid sloshing. Several numerical techniques such as finite difference (FD), Lagrangian finite element (FE), boundary elements, computational fluid dynamics (CFD), Arbitrary-Lagrangian-Eulerian (ALE), and smooth particle hydrodynamics (SPH) have been developed to model water dynamic response.[19,20] For example, ALE modeling has been successfully used in Fluid-Structure Interaction (FSI) analyses[21,22] and proved to be reliable in estimating free surface sloshing and the induced hydrodynamic pressures when compared to experimental results.

The work presented herein is part of a project that aims to advance our understanding of the seismic fluid-structure-soil-interaction in buried water reservoirs using centrifuge tests and numerical modeling. With the lack of available centrifuge experiments that focus on water hydrodynamics, it was deemed important to examine the complex dynamic response of water in a scaled environment under shaking. Moreover, the reliability of numerical models and commonly used analytical and simplified methods in predicting the centrifuge measurements needed to be evaluated as well before upscaling to the full engineering system featuring the components of structure, soil, and water. To this end, this paper encompasses experimental and numerical studies of water sloshing in rectangular containers when subjected to dynamic excitations. A series of five centrifuge model tests were performed where water tanks with a range of dimensions and configurations were subjected to sine waves and earthquake motions (a total of 130 tests) to isolate and investigate the hydrodynamic pressures generated inside the tank. The motions used varied in peak ground acceleration (PGA)

NOVELTY

- A novel series of centrifuge model tests were performed, specifically designed, and instrumented to investigate the hydrodynamic behavior of water and its effects on rigid tanks.
- The reliability and applicability of simplified methods of water hydrodynamics is illustrated.
- The reliability of advanced numerical model in capturing water hydrodynamic behavior is demonstrated.

ranging from 0.003 to 0.74 g, which excited the water at several frequencies, including its natural frequencies. Numerical simulations were performed using the ALE solver in LS-DYNA,[23] a commercial FE package. The numerical models' prediction capability was first tested against available 1 g shake table experimental data and analytical solutions in the literature. Then, the centrifuge experimental data of this study were employed to validate the numerical predictions under a scaled environment. Commonly used analytical, simplified, and code-based methods were also compared to determine their reliability when used in quantifying water dynamic response. The results show that the ALE models yield a good match to the experimental recordings. The analytical and simplified solutions showed reasonable performance under earthquake motions. However, the analytical solutions were found to overestimate the dynamic response when resonance is present. The simplified solutions were also found to underestimate the peak response when sloshing is significant.

2 | ANALYTICAL AND SIMPLIFIED SOLUTIONS

The dynamic behavior of a free liquid surface depends on the type of excitation which can be impulsive, periodic, or random. Many studies have investigated the free and forced sloshing behavior of water by means of mathematical closed-form equations and simplified methods.[4–6] Such solutions are available for different tank properties, excitation types, and motion orientations. With the current state of the practice in retaining structures, many of the simplified methods are being utilized in the design even though the actual field conditions may deviate from their underlying assumptions. Table 1 provides a list of commonly used methods and indicates those being compared in this study. Most of these assume a linear behavior for water and thus might not be applicable for extreme cases where nonlinearity is significant unless they are used to provide preliminary estimates.

2.1 | Closed-form solutions for harmonic excitation

Under external harmonic sinusoidal excitation, the rectangular tank displacement, u, is governed by:

$$u(t) = A \sin \omega t \tag{1}$$

where A is the displacement amplitude, ω is the angular frequency of the sinusoidal excitation, and t is the time. The velocity, $\dot{u}$, of the tank is, therefore:

$$\dot{u}(t) = A\omega \cos \omega t \tag{2}$$

Based on the potential flow theory, the velocity potential, ϕ, satisfies the Laplace equation:

$$\nabla^2 \phi = 0 \tag{3}$$

As discussed in Wu et al.,[26] a linearized solution of ϕ can easily be found from the results of Faltinsen[27]:

$$\phi = A \sum_{n=1}^{\infty} \left[C_n \cos \omega t - \left(C_n + \frac{H_n}{\omega^2} \right) \right] \cos \omega_n t \frac{\cosh k_n z}{\cosh k_n d} \sin k_n \left(x - \frac{l}{2} \right) \tag{4}$$

TABLE 1 List of commonly used analytical and simplified approaches to quantify hydrodynamic behavior.

Approach	Example reference	Input	Output	Application	Compared against			
					[A]	[B]	[C]	[D]
Simplified methods	Westergaard[8]	PGA, γ, d	Peak pressure at the wall	Dam with vertical wall; no convective sloshing				
	Housner[7]	l, d, SA	Maximum base shear and moment	Simple geometries; higher convective modes and nonlinearity are insignificant	X		X	X
	EC8[9]	l, d, SA	Peak pressure distribution	Simple geometries; higher convective modes and nonlinearity are insignificant				
	AWWA D110–13[10]; AWWA D100–21[24]	l, d, SA	Base shear and moment	Circular tanks; higher convective modes and nonlinearity are insignificant	X		X	X
	ACI 350.3–20,[20]	l, d, SA	Peak pressure distribution and wave height	Simple geometries; higher convective modes and nonlinearity are insignificant				
Closed-form solutions	Graham and Rodriguez[4]	l, d, A, ω	Pressure distribution and wave height	Fuel tanks—Sine motions; specific geometry; linear non-resonant problems	X	X	X	X
	Abramson[6]	l, d, A, ω	Pressure distribution and wave height	Fuel tanks in aerospace vehicles—Sine motions; specific geometry; linear non-resonant problems				
	Hunt and Priestley[25]	l, d, $\ddot{u}(t)$	Pressure distribution and wave height	Storage tanks—Linear stepwise motions; specific geometry; small-amplitude wave				
	Wu et al.[26]	l, d, A, ω	Pressure distribution and wave height	Storage tanks—Sine motions; specific geometry; linear non-resonant problems				X
Mechanical Models	Graham and Rodriguez[4]	m_n, h_n, k_n	Global shear force and overturning moment	Commonly used in structural numerical models to represent water as a mass-spring mechanical model	X	X	X	
	Dodge[5]	m_n, h_n, l_n	Global shear force and overturning moment	Alternative to the mass-spring mechanical model				

[A]: Chen and Xue[12]; [B]: Goudarzi and Sabbagh-Yazdi[15]; [C]: centrifuge tests under sine motions; [D]: centrifuge tests under earthquake motions. PGA: peak ground acceleration; γ: water unit weight; l: tank length; d: water depth; SA: spectral acceleration; $\ddot{u}(t)$: acceleration time-series; m_n: impulsive and convective masses; h_n: masses height; k_n: convective springs stiffnesses; l_n: convective pendulum length.

where ω_n is the n^{th} mode natural angular frequency, such that:

$$\omega_n = \sqrt{g k_n \tanh k_n d} \tag{5}$$

x, z, d and l are the horizontal and vertical coordinates, depth of water, and tank length, respectively, as defined in Figure 1. $k_n = \pi(2n-1)/l$, $H_n = 4\omega^3(-1)^n/(k_n^2 l)$, and $C_n = H_n/(\omega_n^2 - \omega^2)$. The dynamic pressure, Δp, can be obtained

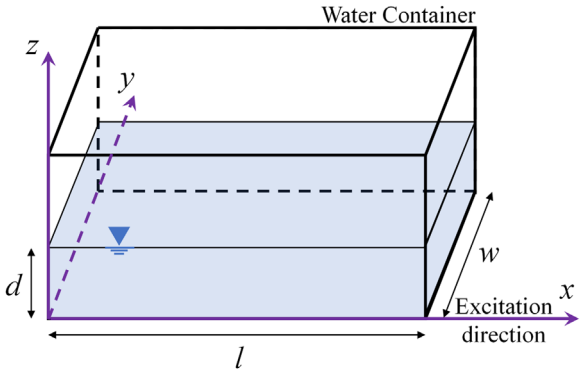

FIGURE 1 The coordinate system of the water container.

through:

$$\Delta p = -\rho\left(\frac{\partial \phi}{\partial t} + \left(x - \frac{l}{2}\right)\frac{d\dot{u}}{dt}\right) \tag{6}$$

where $\rho$is the water density. Solving Equation (6) while given $\dot{u}$ and ϕ in Equations (2) and (4), respectively, yields:

$$\Delta p = -\rho A\left[\sum_{n=1}^{\infty}\left(-C_n\omega\sin\omega t + \left(C_n + \frac{H_n}{\omega^2}\right)\omega_n\sin\omega_n t\right)\frac{\cosh k_n z}{\cosh k_n d}\sin k_n\left(x - \frac{l}{2}\right) - \left(x - \frac{l}{2}\right)\omega^2\sin\omega t\right] \tag{7}$$

Similarly, the free surface elevation, ζ, can then be obtained from:

$$\zeta = -\frac{1}{g}\left(\frac{\partial \phi}{\partial t} + \left(x - \frac{l}{2}\right)\frac{d\dot{u}}{dt}\right)\Bigg|_{z=d} \tag{8}$$

$$\zeta = -\frac{A}{g}\left[\sum_{n=1}^{\infty}\left(-C_n\omega\sin\omega t + \left(C_n + \frac{H_n}{\omega^2}\right)\omega_n\sin\omega_n t\right)\sin k_n\left(x - \frac{l}{2}\right) - \left(x - \frac{l}{2}\right)\omega^2\sin\omega t\right] \tag{9}$$

where g is the gravitational acceleration.

2.2 | Closed-form solutions for random excitation

Hunt and Priestley[25] proposed a set of mathematical equations that described the fluid dynamic response by using small-amplitude wave approximations. The expressions are formulated in such a way that a piecewise continuous acceleration time-history, $\ddot{u}(t)$, of a real earthquake can be used. For rectangular tanks, the dynamic pressure, Δp, can be obtained through:

$$\Delta p = -\frac{\rho}{2}\left[(2x - l)\,\ddot{u}\,(t) + gl\sum_{n=1}^{\infty}\dot{F}_n\,(t)\,\frac{\cosh 2z\alpha_n/l}{\cosh 2d\alpha_n/l}\sin\frac{(2x - l)\,\alpha_n}{l}\right] \tag{10}$$

where $\alpha_n = (2n-1)\pi/2$ and $\beta_n = \sqrt{\alpha_n \tanh 2\alpha_n d/l}$. $\dot{F}_n(t)$ is computed such that:

$$\dot{F}_n\,(t) = \frac{2(-1)^n}{\alpha_n^2\beta_n}\sqrt{\frac{l}{2g^3}}\sum_{p=1}^{M-1}\frac{\ddot{u}\,(t_{p+1}) - \ddot{u}\,(t_p)}{t_{p+1} - t_p}\left[\sin\beta_n\sqrt{\frac{2g}{l}}\,(t - t_p) - \sin\beta_n\sqrt{\frac{2g}{l}}\,(t - t_{p+1})\right] \tag{11}$$

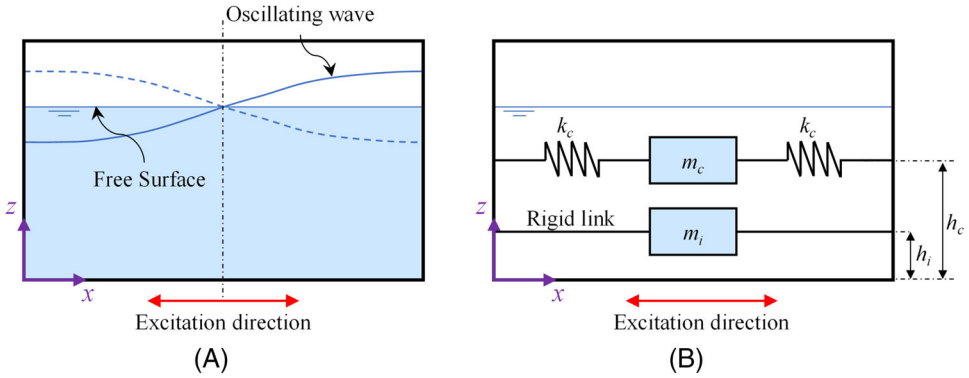

FIGURE 2 Schematic showing (A) slosh wave, and (B) the equivalent mass-spring system in a water tank [after Dodge[5]].

where $t_1 \equiv 0$ and $t_M \equiv t$. The equation of the free surface elevation, ζ, is:

$$\zeta = \frac{2x - l}{2g}\ddot{u}(t) + \frac{l}{2}\sum_{n=1}^{\infty}\dot{F}_n(t)\sin\alpha_n(2x - l)/l \tag{12}$$

2.3 | Simplified and code-based methods

In the field of civil engineering, design methods accounting for hydrodynamic loads were first developed in the context of concrete dams; these methods were then extended to and continue to be used in the design of other water retaining structures. Originally, Westergaard[8] solved the pressure distribution on a vertical rigid wall and water displacements during earthquake loading using the elasticity theory for solids. The solutions were derived for dams and assumed harmonic excitation, small displacements, motions with horizontal accelerations less than 0.1 g, a linear system response, rigid non-yielding walls, a rigid base, a smooth vertical face, and an infinite reservoir. The distribution of the peak hydrodynamic pressure with depth is estimated as:

$$|\Delta p|_{\max} = \frac{7}{8}\alpha\gamma\sqrt{d(d - z)} \tag{13}$$

where α is the PGA in g units, and γ is the unit weight of water ($\gamma = \rho g$). Later studies[28–30] introduced adjustment factors to Westergaard's solutions to correct for water reservoir size, excitation period, and wall inclination with all other original assumptions remaining in place. Nevertheless, Westergaard's numerous unrealistic assumptions make this method inapplicable to systems other than dams that still share the components of an enclosed oscillating body of water and a structural boundary. Remarkably, current practices in the design of water retention structures still rely on Westergaard formulation.

Housner[7] proposed a widely used analytical model for rigid tanks in which hydrodynamic pressure is decoupled into impulsive and convective components using a lumped mass approximation. Epstein[31] extended Housner's procedure into a practical design guideline. In this approach, two masses are considered as shown in Figure 2. The mass close to the bottom, mi, represents the impulsive mass of water which is rigidly attached to the tank at height hi. The other mass, mc, attached to the tank at height hc through springs with stiffness kc, corresponds to the fundamental mode of convective oscillation of the water. This model has been widely adopted, with some modifications, in most of the current codes and standards [e.g., 24]. Eurocode 8[9] follows a similar approach while considering the soil-structure interaction, tank flexibility, vertical excitation, and base uplift effects. However, the consideration of these effects is simple and approximate and therefore does not fully capture these interactions.

Simplified approaches are commonly used in combination with the ground motion response spectrum to obtain the peak responses. However, there are no accurate methods to combine the peaks of the impulsive and convective pressures because they are not necessarily in phase with each other. An accepted practice in design codes is to combine them using the square-root-of-the-square summation (SRSS) method[11] with some exceptions using the absolute summation.[9]

TABLE 2 List of commonly used experimental approaches to quantify water dynamic behavior.

Approach	Example reference	Advantages	Disadvantages
1 g Shake Table	Chen and Xue,[12] Goudarzi and Sabbagh-Yazdi[15]	Economic, easy to perform	Scaling effects; Reynolds number is mismatched
Centrifuge	This study	Improved similitude compared to 1 g	Scaling effects; challenges with high frequencies
Full-scale (real scale)	Kaminski and Bogaert[32]	Direct testing of the prototype system	Costly

TABLE 3 Centrifuge scaling factors for relevant physical properties.

Quantity	Units	Scale factor
Length (L)	L	$1/N$
Volume	L^3	$1/N^3$
Mass (M)	M	$1/N^3$
Time (T)	T	$1/N$
Frequency	1/T	N
Acceleration/Gravity	L/T^2	N
Force	ML/T^2	$1/N^2$
Stress/Pressure	M/LT^2	1

3 | EXPERIMENTAL CENTRIFUGE PROGRAM

Most of the physical tests on hydrodynamics found in the literature are 1 g shake table tests. To the authors' knowledge, the series of centrifuge models tested and presented in this paper are the first reduced-scale ones in the field of hydrodynamics. A list of the different experimental approaches to quantify hydrodynamics behavior is presented in Table 2. Five centrifuge tests were performed on the 9 m radius centrifuge at the Center for Geotechnical Modeling (CGM) at the University of California, Davis with the goals of (1) examining the feasibility of exciting different eigenmodes of water oscillations in a reduced-scale model, (2) establishing the feasibility of measuring water pressures and displacements in a centrifuge model test, and (3) obtaining high-quality data towards examining the validity of analytical solutions and numerical investigations. The tests will be referred to as HYE30 to HYE120 in this paper. All dimensions in this paper are in prototype scale unless stated otherwise.

3.1 | Prototype model and similitude rules

Modeling fluid behavior requires that geometric, kinematic, and dynamic similitude be achieved between the model and prototype. The geometric similitude is satisfied when the ratios of the model and prototype dimensions are equivalent. The kinematic similitude is achieved when the ratios of the vectoral forces between the prototype and model are the same.[33] Both geometric and kinematic similitudes are achieved by the scaling laws that govern centrifuge testing. The scaling laws used in centrifuge testing have been summarized in Garnier et al.[34] The relationships between the relevant engineering parameters and the scale factor for gravity, N, are shown in Table 3.

The forces governing all fluid problems are the inertial, gravitational, viscous, surface tension, and elastic compression forces.[35] Typically, the surface tension and elastic compression forces are negligible and can be ignored for tank sloshing problems.[33] The free surface flow in partially filled tanks is dominated by the interaction between inertial and gravitational forces; the Froude number corresponds to the ratio of inertial to gravitational forces. When analyzing the force ratio of the model and prototype scales, it is found that the Froude number of the model is equal to that of the prototype. However, the ratio of inertial to viscous forces, namely, the Reynolds number, has a mismatch of $1/N$. Hughes[35] and others have recognized that for free surface flows, the Froude criterion should be satisfied, and if applicable, all other effects caused by a mismatch should be minimized. The mismatch in the centrifuge still represents an improvement over other tests such as 1 g shake table tests where the mismatch is even greater ($1/N^{3/2}$). Important conclusions and trends have been obtained and derived from 1 g tests with the known limitation in Reynolds number. Therefore, although the centrifuge tests do not

TABLE 4 List of the different configurations used in the centrifuge experiments at model scale (prototype scale dimensions are reported between parentheses in meters).

Test Series Name	Test #	Gravitation acceleration (g)	Tank length (cm)	Water height (cm)	Roof height (cm)	Number of motions
HYE30	01	60	30 (18.0)	10 (6.0)	40 (24.0)	19
	02	60	30 (18.0)	21.2 (12.7)	40 (24.0)	8
	03	40	30 (12.0)	21.2 (8.5)	40 (16.0)	4
HYE90	01	60	90 (54.0)	10 (6.0)	40 (24.0)	15
	02	60	90 (54.0)	20 (12.0)	40 (24.0)	11
HYE90	03	60	90 (54.0)	10 (6.0)	20 (12.0)	18
	04	30	90 (27.0)	10 (3.0)	20 (6.0)	4
HYE120	01	60	120 (72.0)	10 (6.0)	40 (24.0)	17
	02	60	120 (72.0)	20 (12.0)	40 (24.0)	13
HYE120	03	60	120 (72.0)	10 (6.0)	20 (12.0)	10
	04	27	120 (32.4)	10 (2.7)	20 (5.4)	1
	05	60	120 (72.0)	18 (10.8)	20 (12.0)	5
	06	60	120 (72.0)	18.4 (11.0)	20 (12.0)	5

achieve perfect similitude, they present an improvement from most other common tests and can potentially elucidate important patterns that are otherwise omitted. Additionally, the absence of baffles or other energy dissipation devices, in the models tested, minimizes the impact of viscous forces. Using the scaling laws in Table 3, engineering parameters can be converted from model to prototype scale and vice versa.

3.2 | Test setup

Nine different configurations were tested as listed in Table 4. The models consisted of a partially filled rigid modular water tank where the tank length, tank height, and water height were changed throughout testing. The models were subjected to a range of ground motions applied at the base of the container. Most of the models were spun at a gravitational acceleration of 60 g (e.g., $N = 60$). However, some models were tested at different gravitational accelerations to compromise between the targeted prototype dimensions and excitation frequencies while avoiding the fundamental frequencies of the centrifuge arm and any associated prohibitive resonances. The different final configurations and sine motions selected were influenced by the analytical solutions, specifically the eigenmodes of the water [see Equation (5)]. The natural frequencies for the configurations tested are shown in Table 5. The container was designed so that its inner dimensions could be modified, as desired. A schematic and picture of the tank used in the experiments is presented in Figure 3A. The tank walls and bolt spacing were found to be adequate using structural analysis FE models. The tank was attached to a strong floor placed on the shaker of the centrifuge arm, specifically designed to accommodate a broad range of sizes of testing boxes.[36,37] The spatial limitations in the centrifuge arm prevent the tank length from being larger than 120 centimeters in model scale (72 m prototype scale at 60 g). As a result, the model tank was designed with a variable length that could be adjusted from 30 to 120 cm, in 30 cm increments (model scale). Tank length and height were changed throughout testing from 30 to 120 cm and from 10 to 20 cm in model scale, respectively.

Overall, the different models tested had tank aspect ratios that ranged from 0.08 to 0.71 covering a broad range of configurations. An additional benefit that was realized during the modular tank design was the ability to change the tank height. Modifying the tank height can be used to investigate freeboard effects. A freeboard distance, which is the clear distance between the maximum water surface level and the roof, is commonly provided to sustain the stored water quality and to accommodate wave sloshing caused by earthquakes. Therefore, the tank height was designed to range from 20 to 40 cm in model scale.

A vertical 1-inch-thick (model scale) aluminum vertical wall was designed to separate the tank into a testing and non-testing zone whenever the full length of the tank was not utilized. The vertical wall was held in place by fastening its base and sides with brackets which in turn were fastened to the centrifuge container itself. The inside of the testing zone (the

TABLE 5 The computed first three natural periods of water for the different configurations of the centrifuge experiments.

Test ID	Height-to-length ratio	Natural period of water (s)		
		1st	2nd	3rd
HYE30_01	0.33	5.43	2.78	2.15
HYE30_02	0.71	4.86	2.77	2.15
HYE30_03	0.71	3.97	2.26	1.75
HYE90_01	0.11	14.36	5.43	3.83
HYE90_02	0.22	10.71	4.88	3.72
HYE90_03	0.11	7.57	3.45	2.63
HYE90_04	0.11	10.15	3.84	2.71
HYE120_01	0.08	18.98	6.85	4.62
HYE120_02	0.17	13.85	5.79	4.32
HYE120_03	0.08	18.98	6.85	4.62
HYE120_04	0.08	12.73	4.59	3.10
HYE120_05	0.15	14.49	5.88	4.33
HYE120_06	0.15	14.35	5.86	4.33

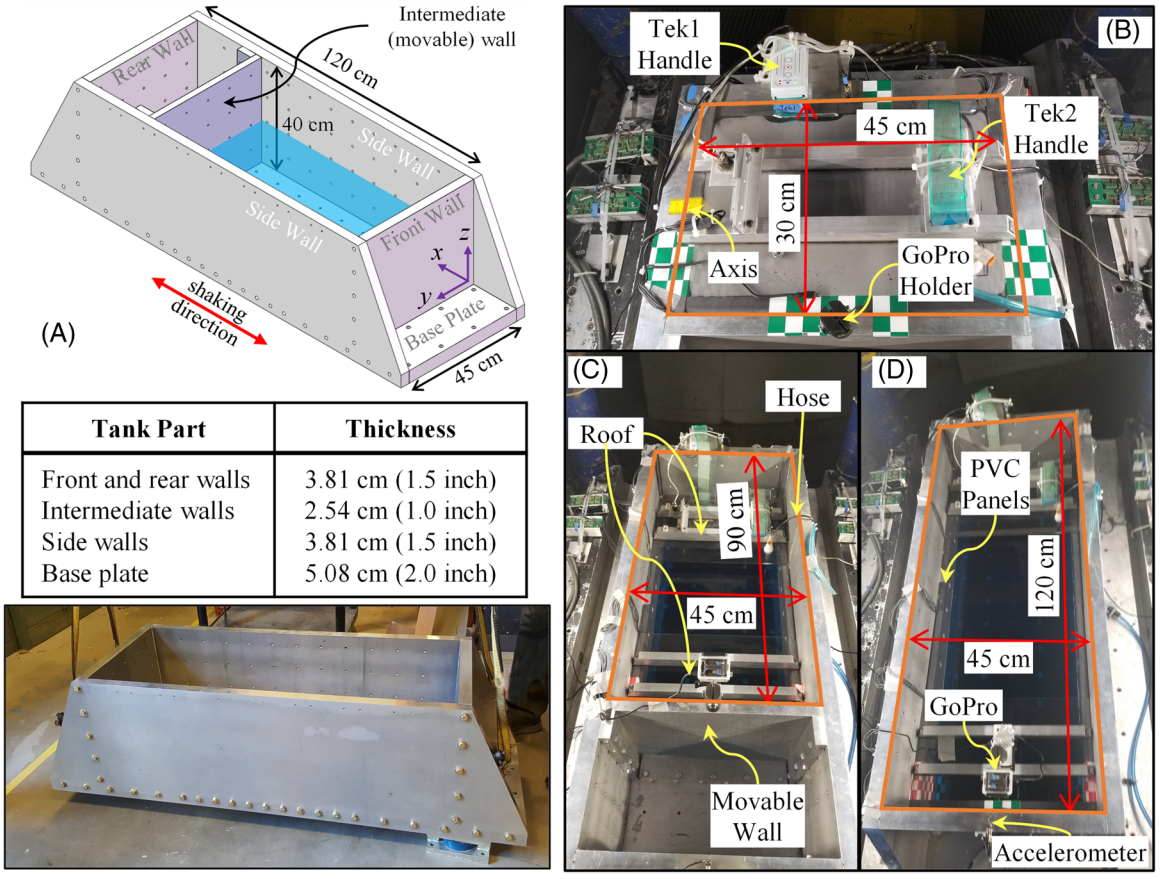

FIGURE 3 (A) The water tank used in the centrifuge experiments. Photos of the water tank in (B) HYE30, (C) HYE90, and (D) HYE120.

water tank) was waterproofed and lined with one-inch-thick polyvinyl chloride (PVC) panels along the walls and base to hold the pressure sensors in place and route their cables to exit the container through several grooves and channels made at the backside of the panels. For configurations where multiple water heights were tested, the tank was filled in flight with a hose. A bulkhead was attached to the roof to which the hose was secured, and water was pumped into the testing zone using the control valve. The desired water height was achieved in flight by monitoring the pressure transducers

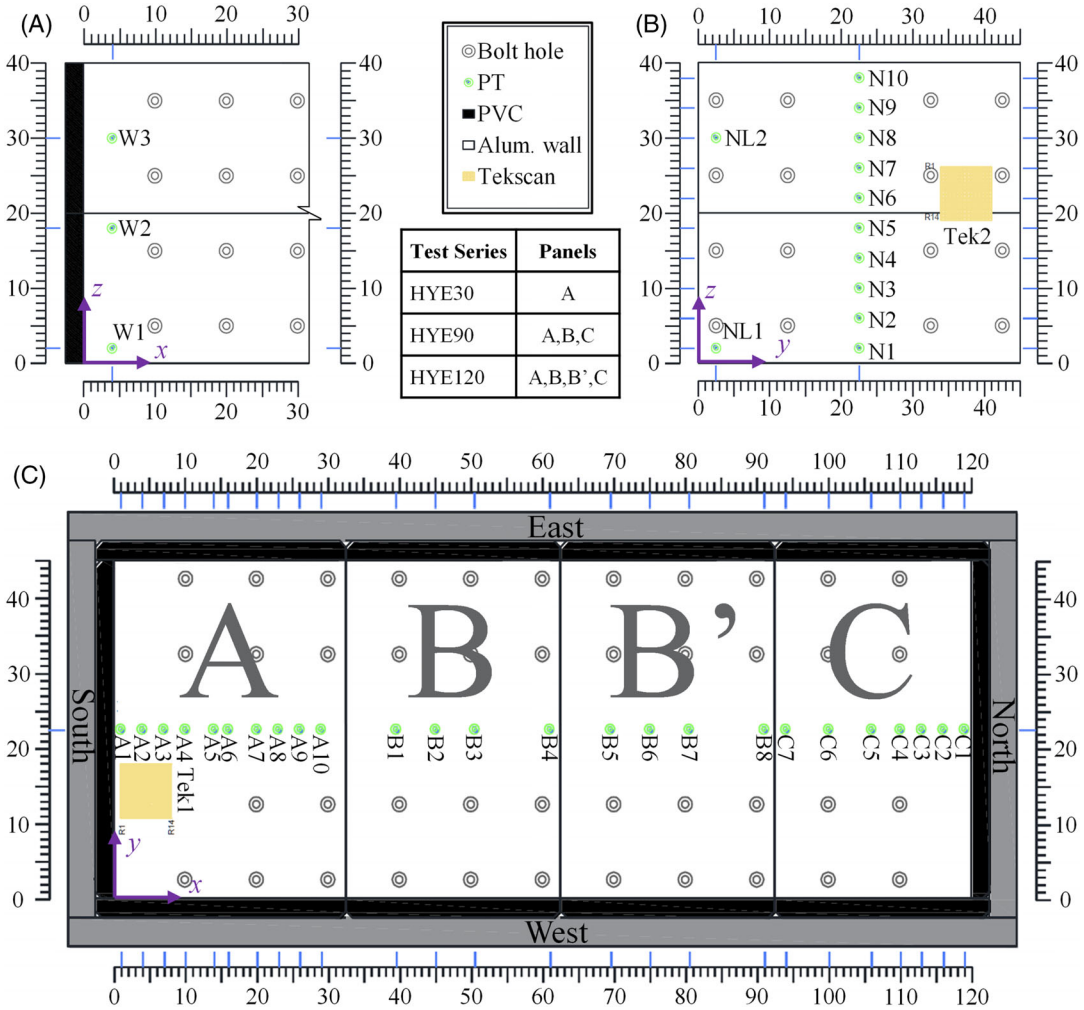

FIGURE 4 Pressure sensor layout of the (A) east wall—Section A, (B) south end wall, and (C) base (all dimensions listed in centimeters of model scale).

and confirmed by measurements taken immediately after the tests. Photographs of the different tank configurations are presented in Figure 3.

3.3 | Instrumentation

Four pairs of piezoelectric accelerometers (oriented vertically and horizontally) were used to measure acceleration at the base and atop tank walls. Two additional pancake accelerometers, one on the east and one on the west side, were located at the base of the container to measure the achieved base acceleration for a given motion. The accelerometer data were recorded at a sampling rate of 5000 Hz. The input acceleration was baseline corrected and filtered using a fourth-order Butterworth bandpass filter with corner frequencies 0.12 and 5.2 Hz (prototype scale).

Waterproofed MS5407-AM pressure transducers (PTs) were utilized as the main pressure recording instrument for the test. The PTs were placed in selected locations on the tank base and walls. Figure 4 illustrates the sensor layout inside the tank (note: the roof and non-instrumented panels are excluded for clarity). The maximum number of pressure transducers for a single test was 48, corresponding to the number of channels available on the centrifuge data acquisition system. The pressure transducers' response was corrected during data processing. The sensors' measurements were offset and filtered. The offset was applied to correct for the sensor creep present before testing started. A zero-delay fourth-order Butterworth low-pass filter was used with the same corner frequency as the one applied to the acceleration measurements. Some sensors failed to work throughout testing. Tactile pressure sensors were also utilized and moved throughout testing, to

TABLE 6 List of the sine motions used in the centrifuge experiments (under 60 g).

Motion ID	ω (rad/s)	Period (s)	Amplitude (m)	No. of cycles
Sine01	6.28	1.0	0.083	3–5
Sine02	4.19	1.5	0.186	3
Sine03	3.77	1.67	0.014	10
Sine04	3.14	2.0	0.128	5
Sine05	2.92	2.15	0.023	10
Sine06	1.15	5.46	0.074–0.185	3–30
Sine07	1.09	5.76	0.092–0.179	3–30
Sine08	1.05	5.98	0.041–0.165	3

measure the pressures along the base, wall, and roof of the container. Two 9500 Tekscan tactile pressure sensors (up to 4000 samples per second) with a nominal capacity of 5 psi were utilized to complement the recorded response from the PTs. The Tekscan readings were calibrated in accordance with Gillis et al.[38] An attempt was made to monitor the water level by using 240 frames per second cameras and coloring the water to increase the contrast. However, the camera's resolution and sampling rate were not adequate to capture the rapid water response.

3.4 | Input motions

A broad range of motions was selected to be applied as inputs to the centrifuge model tests. The motions were applied through two shakers located on the west and east side of the model. The motions can be broadly separated into sine wave and earthquake motions. The sine waves were used to directly compare against theoretical solutions and to induce resonance sloshing. Table 6 shows the characteristics of the sine motions used in the centrifuge tests. For the sine wave sloshing-inducing motions, the predominant frequency of the motion matched the frequency of the water inside the tank. The amplitude of these motions was significantly lower than the non-sloshing motions to avoid engaging the resonant frequencies of the centrifuge arm, 5 and 19 Hz, for the first and second modes respectively.[39] The natural frequency of the centrifuge arm was close to the fundamental frequency of the water itself which ranges from 2 to 12 Hz, depending on the testing configuration. Motions with frequencies lower than 10 Hz were not used as these were too close to the natural frequency of the centrifuge arm.

The earthquake motions were chosen to cover a variety of characteristics (frequency content, duration, acceleration, and evolutionary intensity measures) such as those representatives of faulting mechanisms along the U.S. West Coast. The selection and scaling of the earthquake motions were guided by the ASCE 7−16 design spectra and the 2014 U.S. Geological Survey Hazard maps for the San Francisco region. A list of the selected earthquake motion recordings is presented in Table 7. A significant number of motions from previous centrifuge tests scaled well against the design spectra such that no additional motions were considered. Two new motions from subduction zone earthquakes were selected and implemented to use in the centrifuge tests. The two subduction zone motions were from the 2010 Maule (Mw 8.8) earthquake in Chile and the 2011 Tohoku (M_w 9.0) earthquake in Japan from the recording stations El Roble and IWT008, respectively. Subduction zone motions were of interest because of their relevance to cities such as Seattle, Washington, and its proximity to the Cascadia Subduction Zone. The new motions were implemented in the centrifuge actuator system following the procedure outlined by Mason et al.[40] The procedure removed unwanted frequencies near the first two eigenvalues of the centrifuge arm and removes high frequencies that exceed the capabilities of the shakers. The final achieved motions covered a broad range of characteristics (e.g., see Figure 5) while at the same time honoring the design spectra and relating to the water behavior.

4 | NUMERICAL MODELING

Water sloshing behavior was numerically modeled using the ALE solver available in LS-DYNA. LS-DYNA is a versatile FE simulation platform with advanced modeling capabilities to represent fluid (e.g., water) including ALE.[21] Although a Lagrangian formulation is available, it was shown[19] that the ALE formulation better captures the water behavior, especially

TABLE 7 List of the recorded earthquake motions used in the centrifuge experiments.

Event	M_w	Mechanism	Station	Motion ID	V_{s30} (m/s)	PGA (g)	Arias (m/s)	$D_{5\text{-}95}$ (s)
Landers (1992)	7.4	Strike Slip	Joshua Tree	JOS090	379.32	0.27	2.30	27.10
			Lucerne	LCN260	1369.0	0.28	7.00	13.80
Superstition Hills (1987)	6.5	Strike Slip	Parachute Test Site	BPTS315	348.69	0.58	3.70	11.00
Loma Prieta (1989)	6.9	Reverse Oblique	Saratoga Valley	WVC270	347.90	0.36	1.30	11.10
			Santa Cruz Obser.	LOB090	713.59	0.62	2.70	9.70
Northridge (1994)	6.7	Reverse	Newhall W Pico	WPI046	285.93	0.65	1.50	8.80
			Rinaldi Receiving	RRS228	282.25	0.54	7.50	9.10
			Sylmar Converter	SCS052	251.24	0.37	6.00	15.10
ChiChi (1992)	7.6	Reverse Oblique	TCU078	TCU078	443.04	0.45	5.80	26.10
Kobe (1995)	6.9	Strike Slip	Takatori	TAK090	256.00	0.46	8.70	11.30
Maule (2010)	8.8	Megathrust	Cerro El Roble	MUL090	1951	0.11	0.41	32.65
Tohoku (2011)	9.0	Megathrust	IWT008	IWT008	~1086	0.12	0.35	41.67

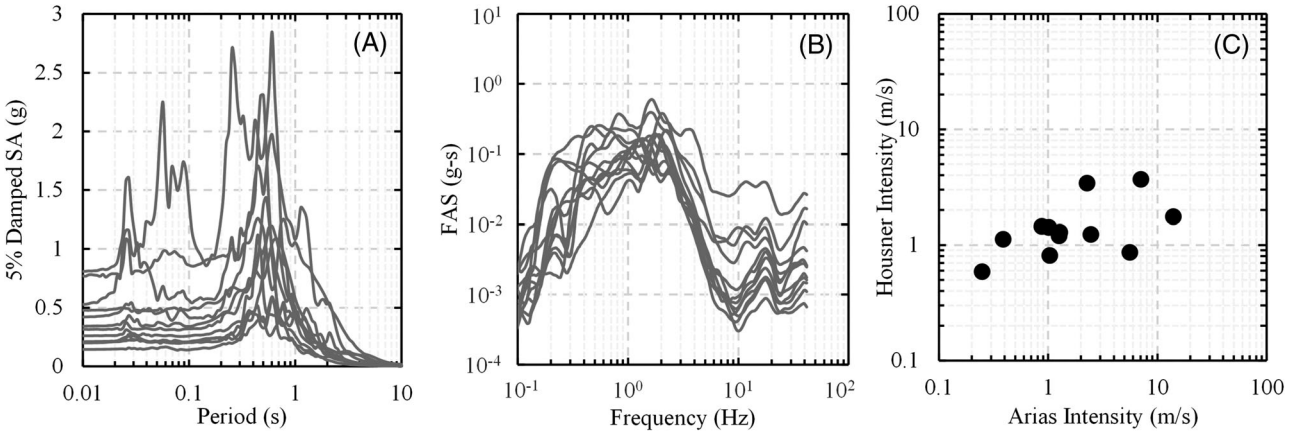

FIGURE 5 Achieved ground motion in the centrifuge testing program (HYE30-01): (A) 5% damped spectral acceleration (SA); (B) smoothed Fourier amplitude spectra (FAS), and (C) Arias and Housner Intensities.

with problems involving high distortions. Kozak et al.[19] conducted analyses with LS-DYNA examining the influence of different numerical formulations on the wave height and sloshing frequency and showed the superiority of ALE over Lagrangian formulations. The commonly used numerical methods for quantifying water behavior are listed in Table 8.

4.1 | ALE models description

Arbitrary Lagrangian-Eulerian (ALE) is an FE formulation that solves the fluid equations on a grid that is partly moving and partly fixed.[42] That is, ALE follows a computational system that is neither attached to the material (Lagrangian-type FE formulation) nor fixed in space (Eulerian-type FE formulation). Therefore, it resolves many of the shortcomings that the traditional Lagrangian- and Eulerian-type FE simulations have. The idea stems from the fact that a Lagrangian formulation should be adopted where boundaries move, while a Eulerian point of view should prevail where deformations are large.

Nonlinear explicit FE ALE models were developed using LS-DYNA to capture the transient and nonlinear water behavior after the initiation of the motion until the end of the test. In this study, a slice model of the tank was considered since a unidirectional motion was applied, the conditions were uniform along the tank width, and the three-dimensional effects were rather insignificant. The slice model was composed of the tank walls and floor, water, and air in prototype scale. Since the tank walls used in the experiments were relatively stiff, they were represented by rigid four-node Lagrangian shell elements. The water, and surrounding air, was modeled using ALE eight-node brick elements. The ALE domain

TABLE 8 List of commonly used numerical approaches to quantify hydrodynamic behavior.

Approach	Example reference	Advantages	Disadvantages
Lagrangian FE	Doğangün et al.[41]	Computationally efficient; easy to define model boundary	Inaccurate at high distortions
ALE	Donea et al.[42]	Multi-material interaction; capture high distortions	May exhibit leakage problems
SPH	Monaghan[43]	Mesh-free; can model high distortions	Difficulties in defining model boundary; limited in capturing pressures and free surface
CFD FV	Chen and Xue[12]	Can capture breaking waves	High computational cost

ALE: Arbitrary Lagrangian-Eulerian; CFD: computational fluid dynamics; FE: finite element; FV: finite volume; SPH: smoothed-particle hydrodynamics.

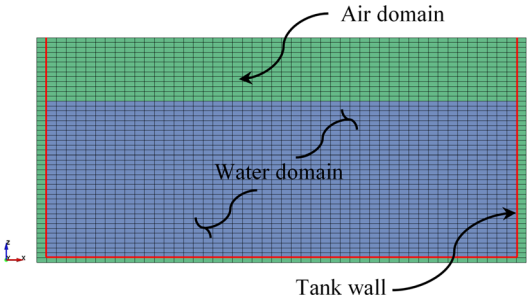

FIGURE 6 Example of a water tank ALE model.

requires defining two materials (e.g., water and air) that interact together through the ALE background mesh as shown in Figure 6. A single ALE mesh can thus be occupied by more than one material. To take full advantage of the ALE formulation, a prescribed motion, the same as the input/tank motion, was applied to the background mesh to have accurate readings at points of interest. A slip condition was assigned to the out-of-plane boundary, and a constant downward gravitational acceleration of 9.81 m/s^2 was applied throughout the simulation. No damping was applied.

Coupling between the tank and water was established using the *CONSTRAINED_LAGRANGE_IN_SOLID feature available in LS-DYNA. The coupling prevents the water from penetrating the tank shell by applying counter normal forces while allowing slippage. The *MAT_VACUUM material model was adopted to model air with a negligible density. *MAT_NULL, as a constitutive model, and *EOS_GRUNEISEN, as the equation of state (EOS), were used to describe the water material. The Grüneisen equation of state was used to describe the relationship between the total pressure, p, and the volume of water with the general form of[21]:

$$p = \frac{\rho_0 C^2 \mu \left[1 + \left(1 - \frac{\gamma_0}{2}\right)\mu - \frac{a}{2}\mu^2\right]}{\left[1 - (S_1 - 1)\mu - S_2 \frac{\mu^2}{\mu+1} - S_3 \frac{\mu^3}{(\mu+1)^2}\right]^2} + (\gamma_0 + a\mu)E \tag{14}$$

where $\mu = (\rho - \rho_0)/\rho_0$, ρ_0 and ρ are the initial and current densities of water, respectively, C is the sound velocity of the material, S_1 to S_3 are unitless material coefficients, γ_0 is the unitless Grüneisen gamma, a is the first order volume correction to γ_0, and E is the internal energy per unit volume. The water material and EOS parameters used in the models are presented in Table 9, based on data obtained from Hertel.[44] In order to ensure the results' independence from the mesh size, a mesh sensitivity analysis was conducted to determine the optimal mesh size or number of mesh elements in the simulation. Python scripts were employed to automate the post-processing of LS-DYNA results.

TABLE 9 Water material properties and related Grüneisen EOS parameters.

	Material properties		Grüneisen EOS parameters					
Material parameter	Density (kg/m^3)	Dynamic viscosity (Pa.s)	C (m/s)	S_1	S_2	S_3	γ_0	a
Value used	1000	8.9×10^{-04}	1647	1.921	-0.096	0	0.35	0

4.2 | Numerical predictions

The ALE prediction capabilities were first examined against unidirectional 1 g shake table experiments available in the literature and the closed-form solutions presented earlier. This step was essential in order to verify that the formulation can give an accurate prediction of the water behavior under normal gravitational conditions before moving forward to the centrifuge scaled tests. Then, the centrifuge tests of this study were numerically simulated, and the results were compared. The results were also compared with the analytical[25,26] and simplified solutions[8,9,11] where applicable (see Table 1).

4.2.1 | 1 g shake table experiments

Chen and Xue[12] carried out a series of experiments on a partially filled rectangular tank excited by a motion simulation platform. Pressure probes were placed along the tank wall height to measure the hydrodynamic pressures. Their experimental results were used in this study to validate the pressure outcome of the ALE models. The pressure obtained from a given ALE mesh element was the weighted average pressure of the materials occupying that element, as per the equation below:

$$p = \sum_{i=1}^{m} (VF_i p_i) \tag{15}$$

where m is the number of materials (in this case, $m = 2$) and VF_i is the volume fraction of the material i. The volume fraction is the ratio of the volume of the material occupying a certain ALE mesh element with respect to the mesh element's total volume. For instance, the volume fraction of the water, VF_w, is unity ($VF_w = 1$) if the FE mesh (background ALE element) is filled entirely with water, $VF_w = 0$ if the element is filled entirely with air (void), and $0 < VF_w < 1$ if the element volume is partially filled with water. However, since the pressures were obtained at the sensors' locations which were fully submerged ($VF_w = 1$) and the ALE mesh motion followed that of the tank, the pressure obtained from the ALE elements was the same as the water pressure. Figure 7 shows the comparison of the water hydrodynamic pressures of two cases. The experimental, analytical, and numerical results showed good agreement with the simplified methods underestimating the peak responses.

Another series of shaking table experiments on a rectangular tank filled with water was conducted by Goudarzi and Sabbagh-Yazdi[15] to investigate the nonlinear behavior of liquid by inducing high amplitude sloshing. The behavior was measured by recording the sloshing free surface elevation. In this study, the tank dimensions and the sine motions of two cases used in the experiments were reproduced numerically in LS-DYNA. Since the background mesh of the ALE is not attached to the material points, as in the Lagrangian-based formation, the water surface height time history cannot be readily obtained from nodal displacements. Therefore, an alternative technique was utilized to calculate the wave height time history using the water volume fraction, VF_w. As shown in Figure 8, the VF_w was extracted for a column of mesh elements near the measurement location at each time step of the analysis. Then, the free surface elevation, ζ, was calculated as follows:

$$\zeta = \sum_{j=1}^{e} \left(VF_{w,j} h_j\right) - d \tag{16}$$

where e is the total number of mesh elements in the extracted column, and h is the height of the mesh element j. It is noteworthy that, despite the ALE simulation's capability for mesh deformation, the size and shape of the mesh were deliberately kept fixed during the simulation. This decision was taken to ensure that the output results from the background

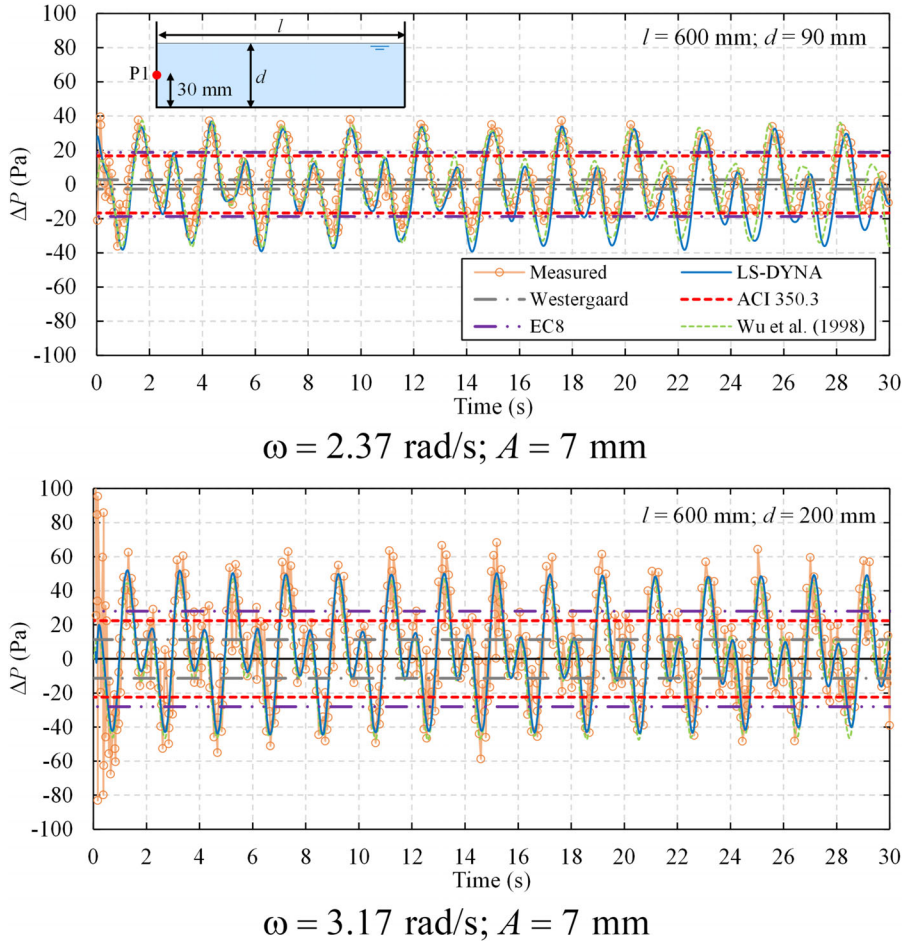

FIGURE 7 Hydrodynamic pressures at P1 under sine motions in 1 g shake table experiments.[12].

mesh elements represented stationary points with respect to the tank. Further, the background mesh already adequately covered the entire space inside the tank, where water sloshing occurs.

The comparison of solutions from different methods is provided in Figure 8. The results showed good agreement with some small discrepancies. However, it can be overall noticed that the analytical solution of Wu et al.[26] tended to underestimate the wave height for resonance or when the sloshing wave height was large [e.g., Figure 8A].

4.2.2 | Centrifuge experiments

Preliminary numerical models were developed before performing the centrifuge physical model tests to provide Class A predictions, as defined by Lambe,[45] which helped in improving the experimental design setup. After carrying out the centrifuge experiments, the five centrifuge tests, defined in Table 4, were reproduced numerically in prototype scale using the ALE formulation to provide Class C and C1 predictions. The conversion from the model to the prototype scale followed the scaling law presented in Table 3. The achieved sine wave and earthquake motions were applied on the tank as acceleration time histories, and the water pressures were obtained at the locations of the sensors. The water sloshing height was not evaluated since it could not be measured during the experiments. Yet, validating the computed water pressure would suggest that calculated water height should also compare favorably with the experimental results.

The computed hydrodynamic pressure is the sum of contributions of the convective and impulsive modes of water; however, a numerical evaluation of these contributions separately is not possible. Yet, it is understood that the impulsive mode would dominate the behavior when water is subjected to high-frequency earthquake motions. On the other hand, low-frequency sine-wave motions, especially those with frequencies close to the natural frequencies of water, would excite the convective mode of water. Therefore, exercising the ALE model on both types of motions would evaluate its capability

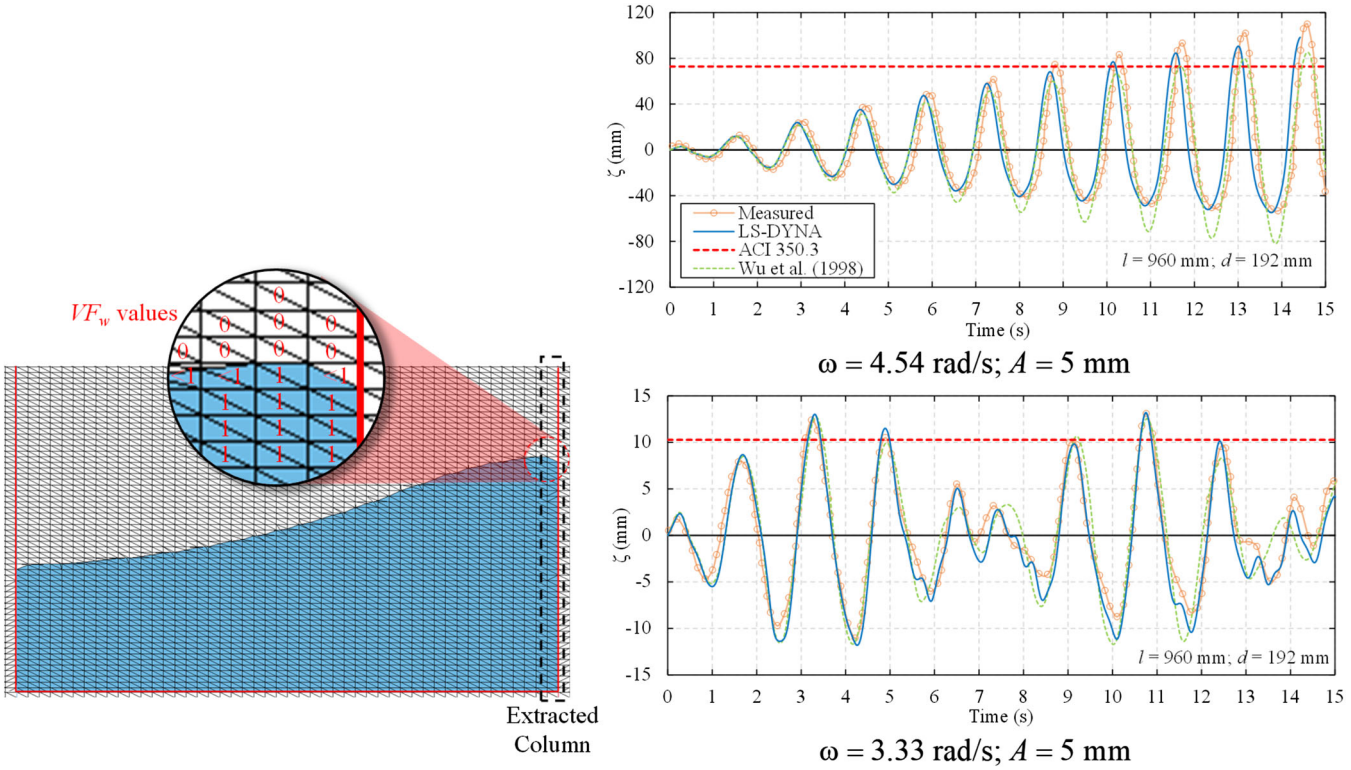

FIGURE 8 Free surface elevation time history calculated from volume fracture of water under sine motions in 1 g shake table experiments.[15]

of capturing the different behavioral modes of water. In general, it is observed that the numerical prediction satisfactory matches the experimental results in all 130 tests. Examples are presented in Figures 12 and 13, which show the comparison of measured and computed water pressures along with the analytical and simplified solutions when subjecting the tank to sine and earthquake motions, respectively.

5 | DISCUSSION

The numerical ALE models showed a good performance in reasonably reproducing the outcome of all the experiments. Under sine motions, the numerical models were able to capture the water response in terms of water pressure and free surface elevation as shown in Figures 7–9. Also, it is observed from Figure 9 that the natural modes of the water body were well represented by the numerical models when applying the scaling laws. For example, a resonance condition was achieved when applying Sine06 motion [see Figure 9A], and continuous sloshing of water was observed after the end of Sine04 motion [see Figure 9C] since the applied sine wave period was close to the natural period of the water body. On the other hand, in Figure 9B, water pressures reverted to hydrostatic once the Sine01 motion ended, although the motion had more cycles and higher PGA (by an order of magnitude) compared to Sine04. The ALE models showed a similar performance when subjecting the tank to earthquake motions as shown in Figure 10. Due to the impulsive nature of earthquake motions, the hydrodynamic pressure generated was similar in shape to the achieved motion acceleration time series. An exception was the case shown in Figure 10A where further sloshing was observed post-earthquake. This is attributed to the coincidence of the 1st mode period with a non-zero spectral acceleration which excited the fundamental convective mode of water. Figure 11 shows a comparison of the measured and computed dynamic pressures at the wall for each timestep of all motions. The smoothed log residual was observed to be low for both earthquake and sine wave motions. The log residual of a parameter of interest, X, is defined as follows:

$$\text{Residual}X = \log\left(\frac{X_{\text{measured}}}{X_{computed}}\right) \tag{17}$$

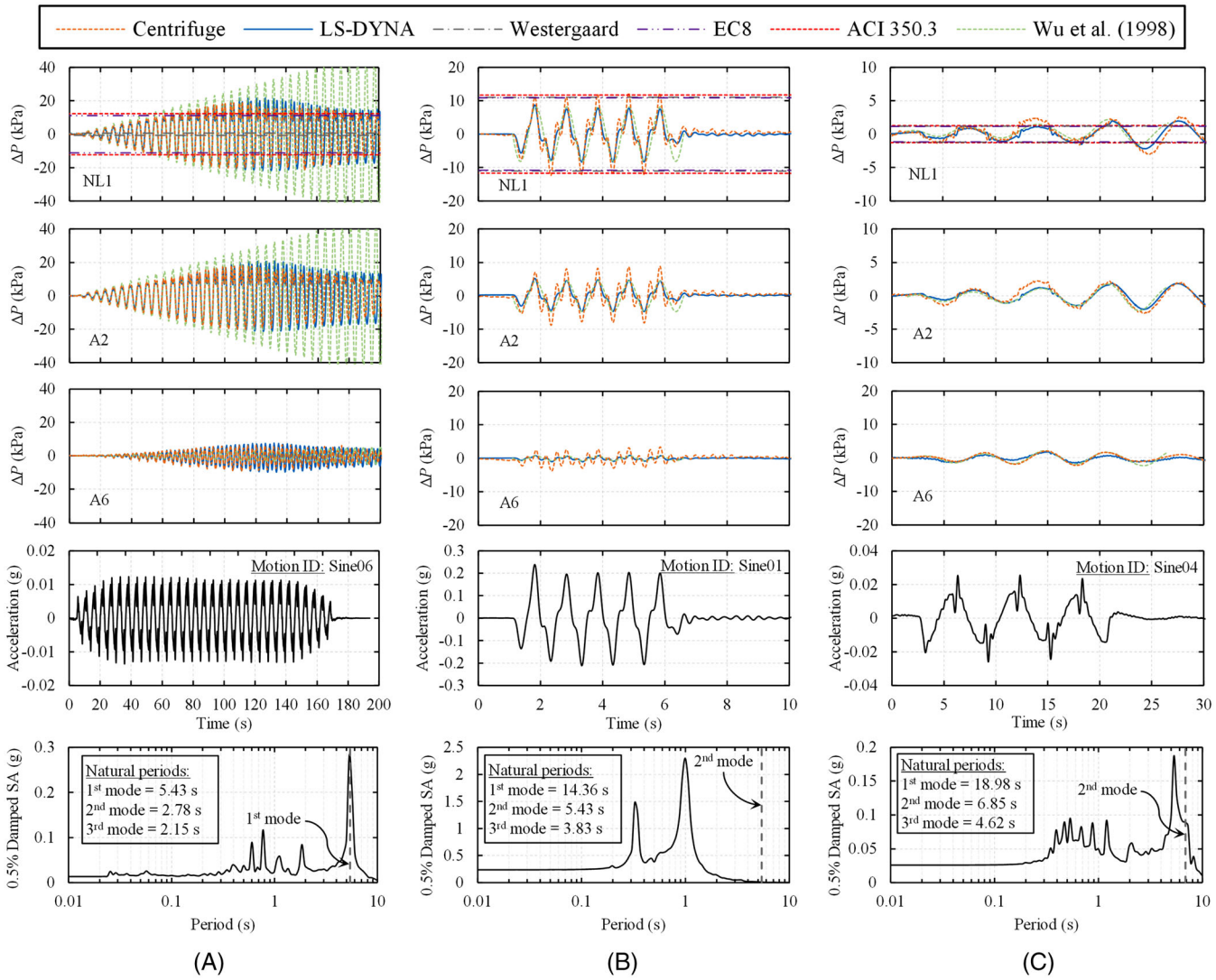

FIGURE 9 Hydrodynamic pressures under sine wave motions in (A) HYE30_01, (B) HYE90_01, and (C) HYE120_02.

A residual greater than zero indicates underestimation while a residual less than zero indicates overestimation. Similar plots for the analytical and simplified solution log residual are provided in Figure 12. The analytical solution showed a good performance with earthquake motions and generally overestimated the peak pressures generated by sine wave motions due to linear theory imposed by the analytical solutions. Due to the relatively large size of water retaining structures, the natural periods of retained water bodies are typically medium to high. This gives rise to the high impact of long duration motions that are dominated with low frequency content which may cause resonance, not to mention the fatigue effects that are imparted on the structure due to the long cyclic hydrodynamic pressures. Water retaining structures tend to be relatively large in size, resulting in natural periods of retained water bodies that are usually medium to high. As a consequence, these structures are more vulnerable to long-duration motions of low-frequency content (high periods), which can lead to resonance. Additionally, the cyclic hydrodynamic pressures during and after (convective sloshing) these long-duration motions can cause fatigue effects in the structure.

When subjected to strong excitation or when close to resonance, nonlinear liquid sloshing behavior exhibits several signs and characteristics that distinguish it from linear sloshing behavior such as (1) asymmetric shape of the free surface with sharper crests and flatter troughs, (2) amplitude-dependent behavior where the natural frequency and behavior of the sloshing system change as the amplitude increases, and (3) wave-breaking and non-sinusoidal wave shapes causing energy dissipation. Such effects cannot be captured by analytical solutions due to their inherent linear assumption. For example, in Figure 8A, the non-symmetry in the wave rises and troughs, due to nonlinearity and base restraint, was not captured by the analytical solution. Moreover, in contrast to the centrifuge and numerical results in Figure 9A, a continuous increase in

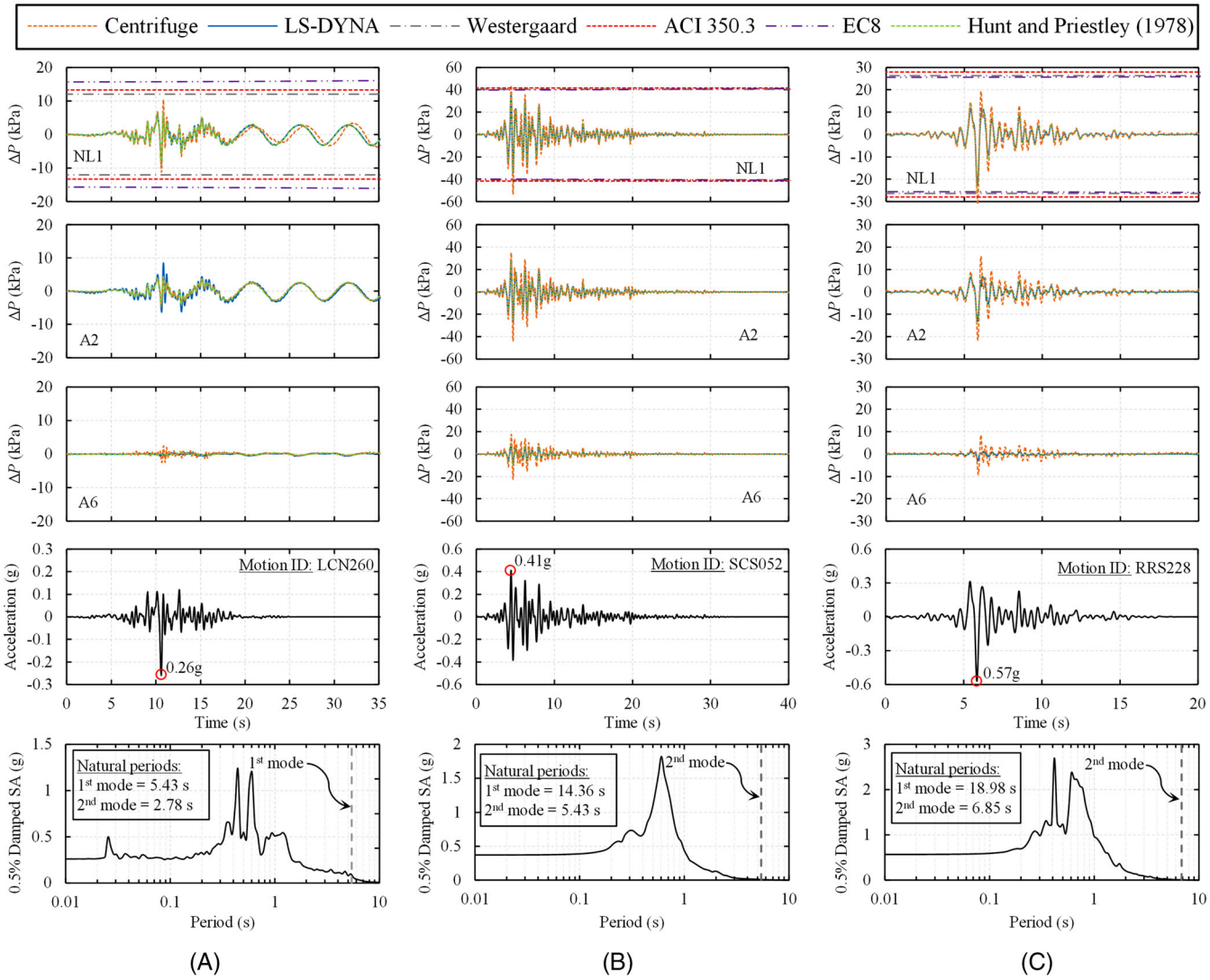

FIGURE 10 Hydrodynamic pressures under earthquake motions in (A) HYE30_01, (B) HYE90_02, and (C) HYE120_02.

dynamic pressure was suggested. On the other hand, simplified solutions were found to generally underestimate the peak responses under sine excitation. This is mainly because Westergaard's solution does not incorporate convective sloshing effects, and EC8 and ACI 350.3 do not account for the higher convective modes of sloshing. On the other hand, when dealing with earthquake motions, the simplified methods yielded lower residuals while ACI 350.3 and EC8 outperformed Westergaard as shown in Figure 12. However, unlike the analytical and numerical methods, they can only provide peak values. It was observed that when convective sloshing was significant, like the case in Figure 10A, EC8 and ACI 350.3 tended to overestimate the peak response because of the added contribution of the convective mode where its peak pressure was not necessarily in phase with that of the impulsive. In that case, EC8 yielded a higher peak pressure compared to ACI 350.3 since it follows an absolute summation instead of the SRSS. It is worth noting that sloshing against the roof was not observed in the centrifuge and numerical models. However, in the event that such a phenomenon occurs, the numerical model can capture its resulting nonlinear behavior and energy dissipation,[19] which cannot be achieved by the analytical or simplified methods.

To better understand the pressure distribution in the tank, Figures 13 and 14 present examples of the distribution of the absolute peak pressures ($|\Delta P|_{max}$), defined as $|\Delta P|_{max} = \max|P\text{-}P_o|$ (P_o, is the initial hydrostatic pressure), on the tank wall and base when subjected to sine and earthquake motions, respectively. In the case of the sine wave motion presented in Figure 13, the vertical distribution shape of the peak dynamic pressures on the wall obtained from the numerical model agreed with the code-based solutions (e.g., ACI 350.3) and passes through the centrifuge data point. In such a case, where the convective mode was dominating, the maximum dynamic pressure occurred at the free surface and decreased with

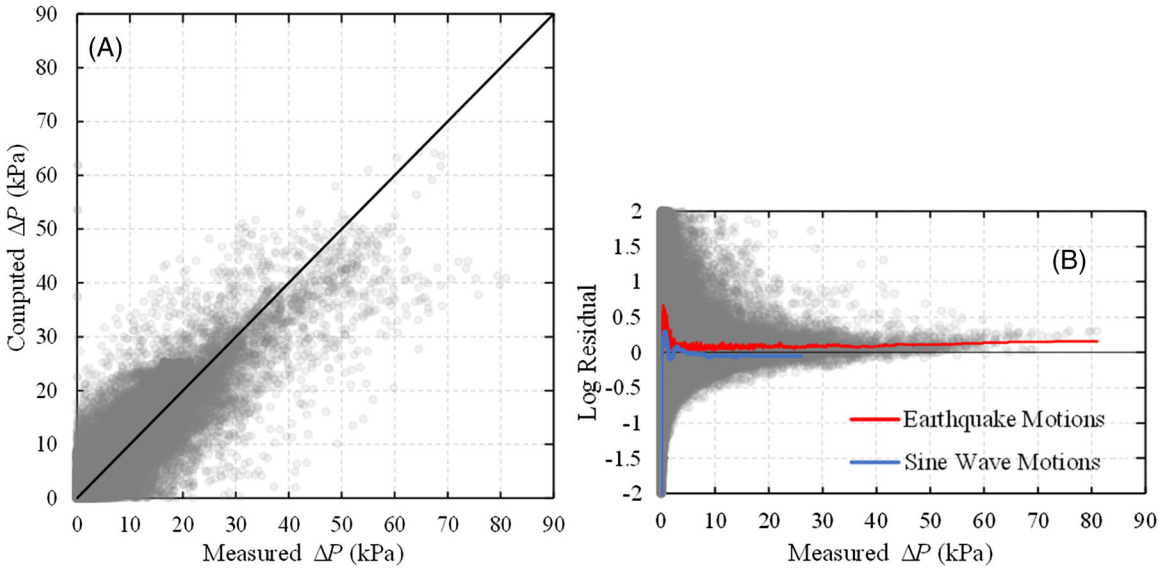

FIGURE 11 Comparison of (A) measured and computed dynamic pressures of all the data points in the time-series at the wall for all motions and (B) their log residuals. Smoothed log residuals are plotted with colored lines.

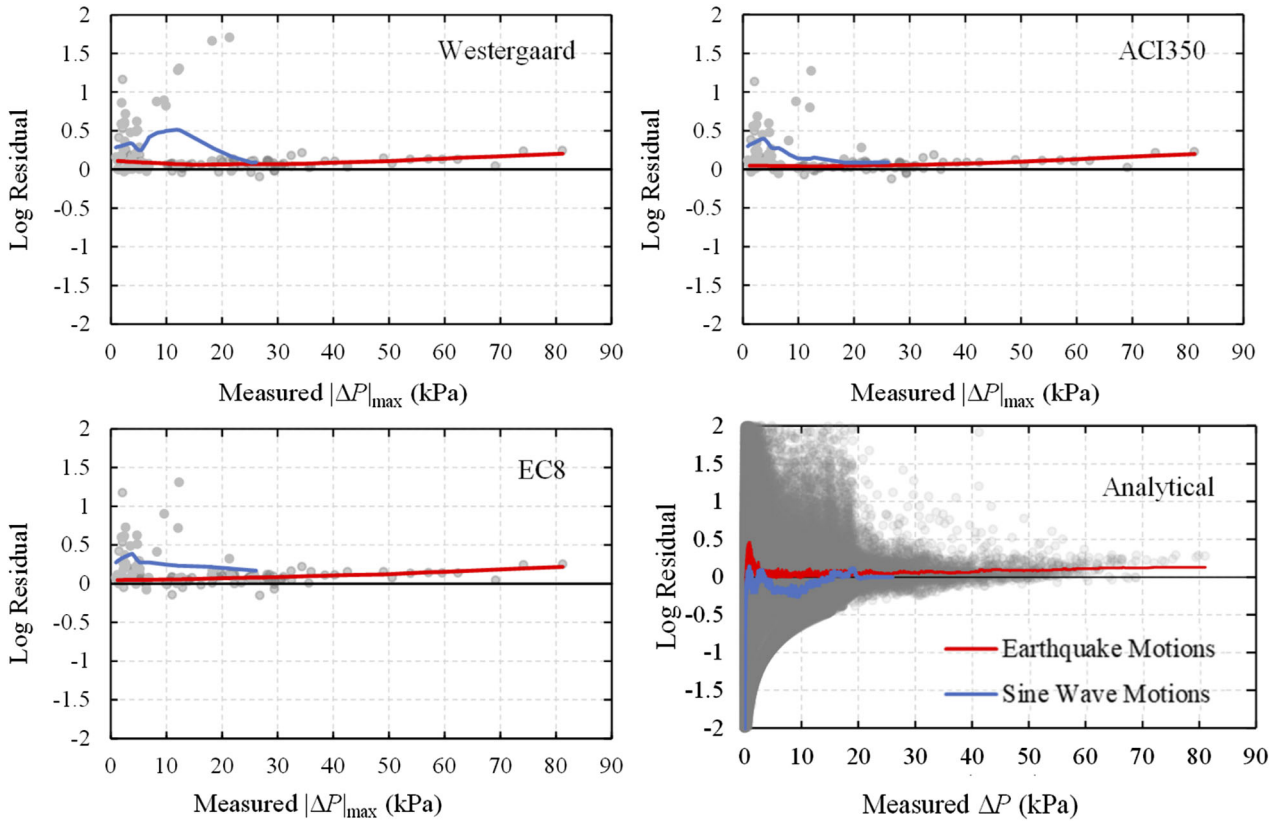

FIGURE 12 Log residuals of measured and computed based on four different approaches dynamic pressures at the wall for all motions.

depth. Also, an increase in pressure was observed across the base with maximum values occurring close to the corner. On the contrary, for the high-frequency earthquake motions presented in Figure 14, the results showed the maximum dynamic pressure on the wall occurring near the base. Moreover, the dynamic pressure at the base was mainly concentrated near the corners and rapidly decreased as moving away from the walls. A comparison of the computed and measured $|\Delta P|_{max}$ at the wall for all earthquake motions is provided in Figure 15 where the numerical models showed the lowest residual.

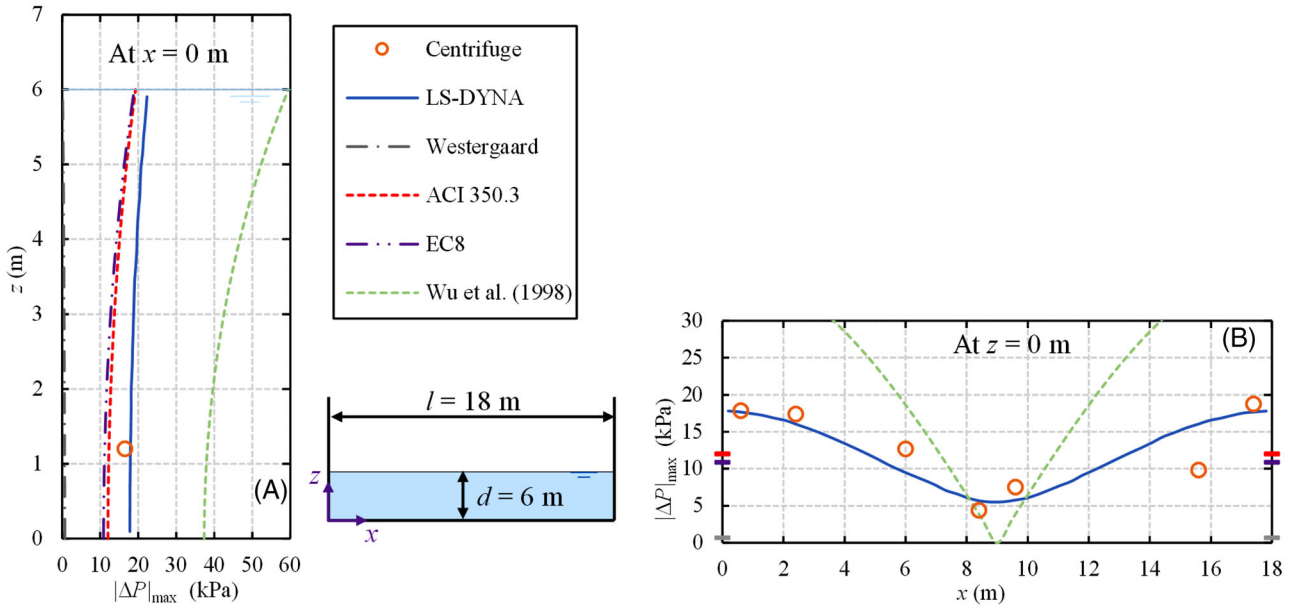

FIGURE 13 The maximum hydrodynmaic pressure distribution on the (A) tank wall and (B) base under the Sine06 (15 cycle) motion in HYE30_01.

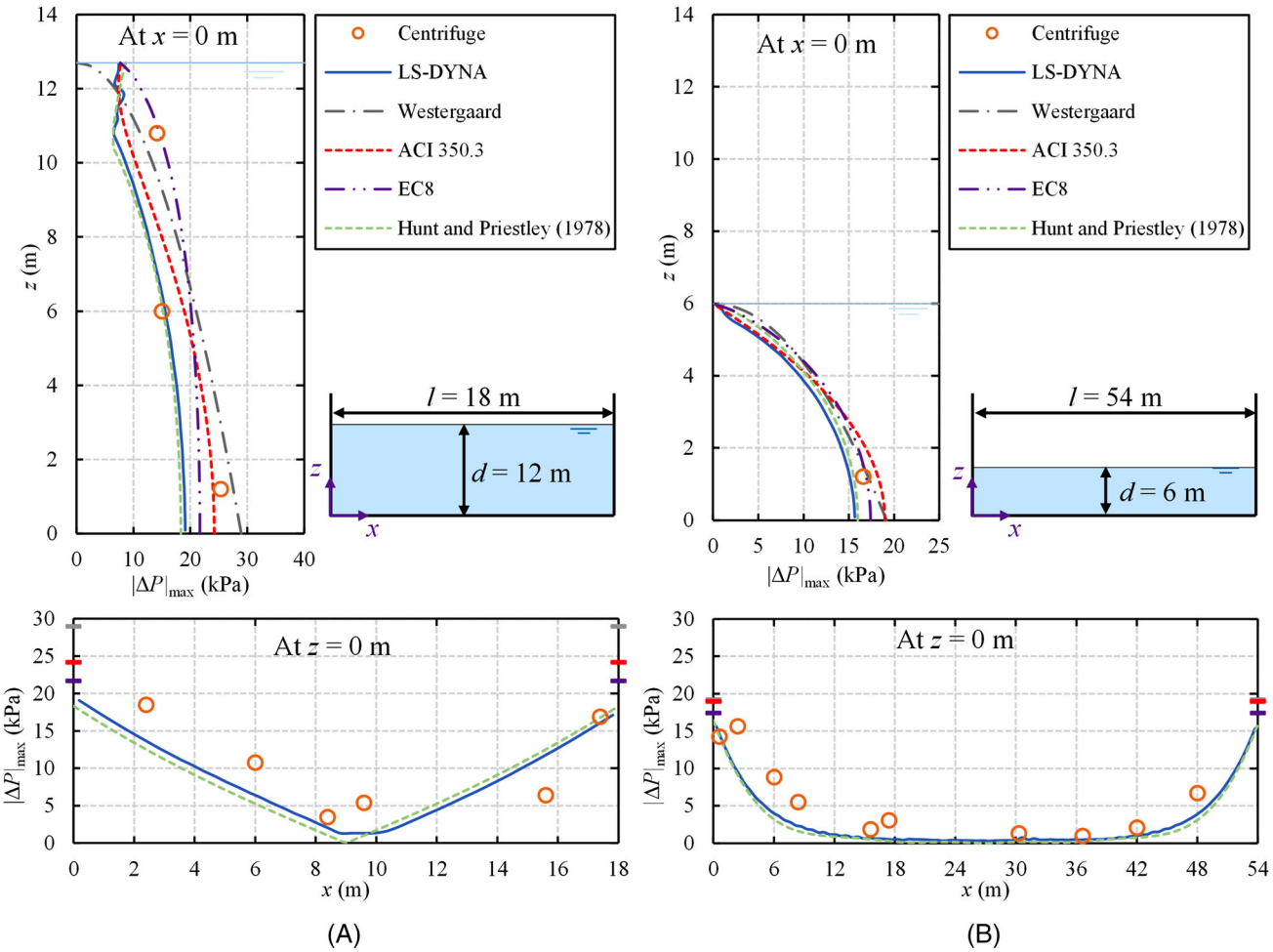

FIGURE 14 The maximum hydrodynamic pressure distribution on the tank wall and base under (A) LCN260 motion in HYE30_02, and (B) SCS052 motion in HYE90_01.

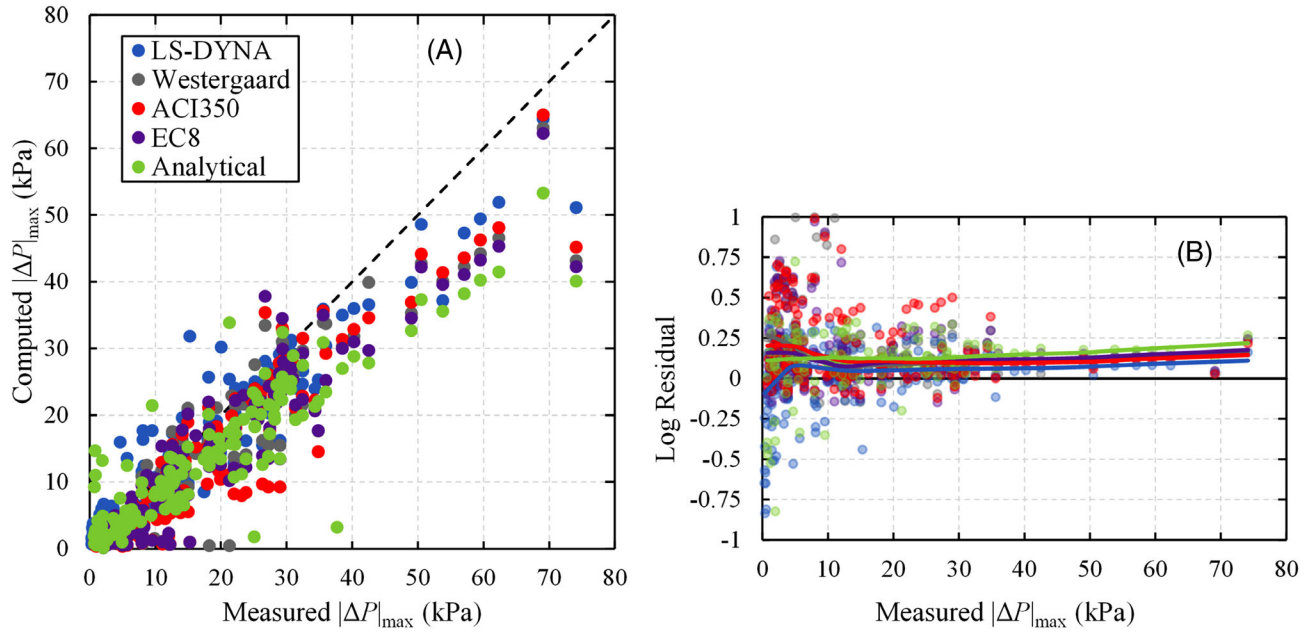

FIGURE 15 Comparison of the (A) computed and measured $|\Delta P|_{max}$ at the sensors located at the wall and (B) their corresponding log residuals.

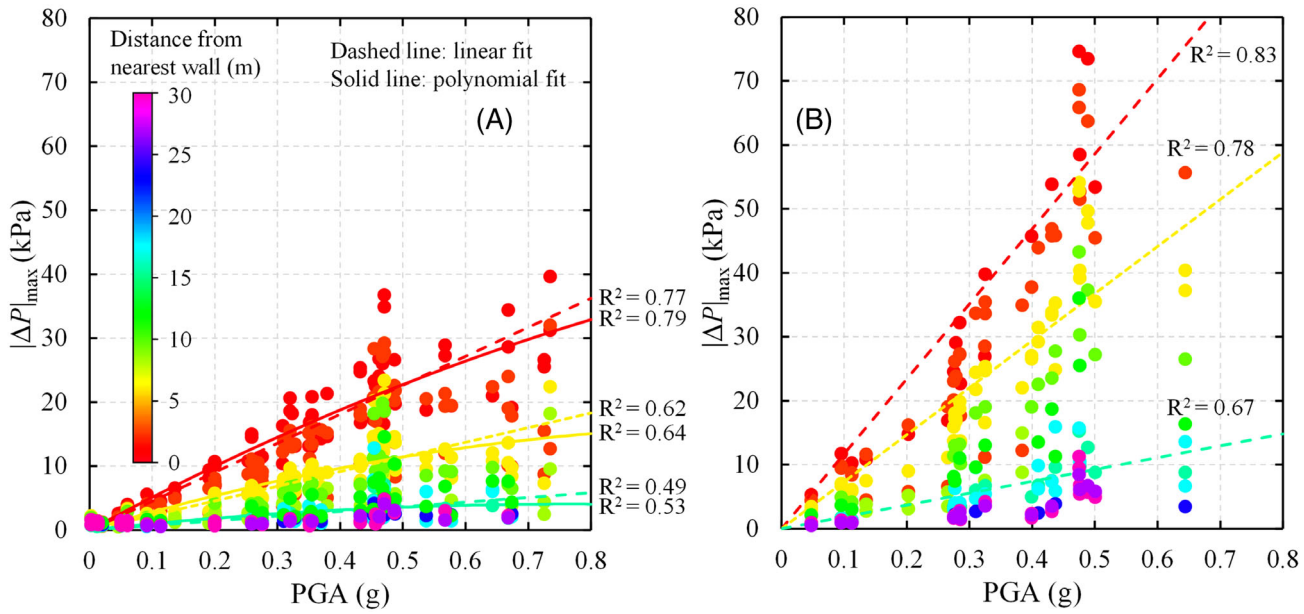

FIGURE 16 Summary plots of the measured $|\Delta P|_{max}$ distribution with the distance from the nearest wall and PGA for (A) 6 m and (B) 12 m initial water height.

The measured distribution of $|\Delta P|_{max}$ with respect to the nearest wall for all earthquake motions are provided in Figure 16. It was observed that high $|\Delta P|_{max}$ values were concentrated near the walls. Also, as the initial water height and PGA increased $|\Delta P|_{max}$ increased. The normalized $|\Delta P|_{max}$ versus PGA at the wall is provided in Figure 17 where the numerical models showed the least residual compared to the other methods. In Figures 16 and 17, a mild nonlinear behavior of water with respect to the applied PGA was observed, where $|\Delta P|_{max}$ deviated from the linear trend beyond PGA values greater than 0.5 g. This contradicts the linear scaling assumption with peak ground parameters, typically followed by simplified methods (e.g., Westergaard).

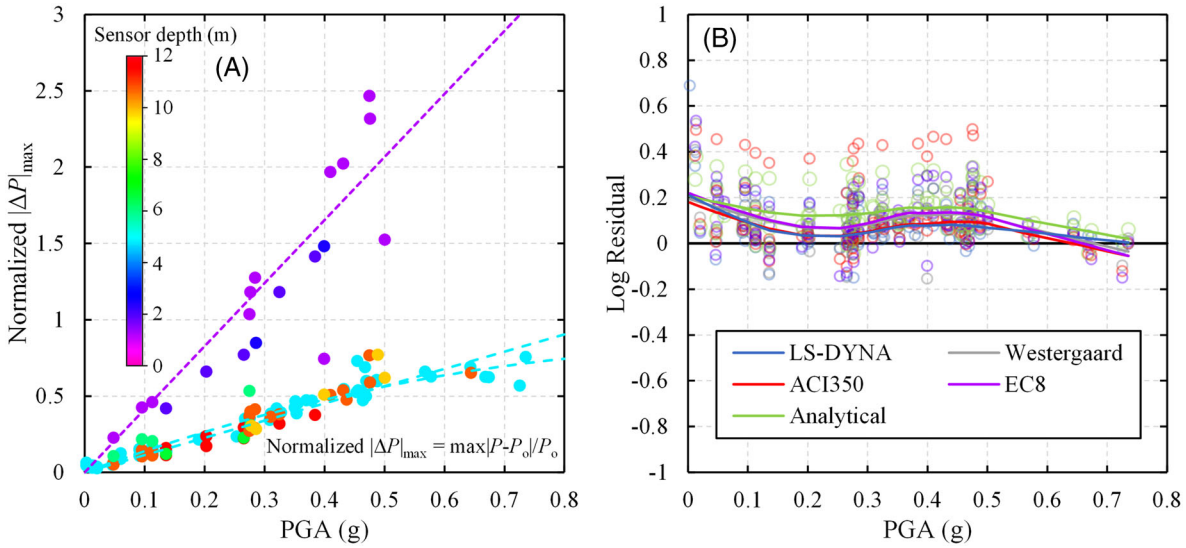

FIGURE 17 The distribution of (A) the measured normalized $|\Delta P|_{max}$ at the wall with depth and PGA and (B) the corresponding log residuals of the computed values.

6 | CONCLUSION

This paper presents a unique series of five centrifuge model tests that investigates the hydrodynamic loading generated in water tanks. The centrifuge models correspond to water tank dimensions ranging from 12 to 72 m in length and 6 to 12 m in water height. The motions used included sine wave and earthquake records and varied in peak ground acceleration ranging from 0.003 to 0.73 g, which excited the water at several frequencies, including its natural frequency. The dataset produced included a total number of 130 cases. Numerical simulations using the ALE solver available in LS-DYNA were then utilized to model the water behavior under external excitation. The numerical models' predictions were first validated in terms of water pressure and wave height against 1 g shake table experiments available in the literature. Then, the centrifuge experiments were numerically reproduced, and the results of the water pressure were compared. Additionally, solutions from analytical and simplified methods were superimposed, and conclusions were drawn on their limitations.

The series of centrifuge models presented in this paper were the first reduced-scale ones in the field of water hydrodynamics. Based on the measurements, a mild nonlinear trend in peak pressure increase was measured beyond PGAs of 0.5 g in contrast to the linear assumption inherent with the simplified solutions. Westergaard's solution of peak pressures reasonably captured the measurements for cases under earthquake motions, however it underestimated for sine motions where water sloshing is significant. EC8 and ACI350.3 reasonably captured the measured peak pressures for cases under earthquake motions and underestimated for sine motions but with better performance than Westergaard. The analytical solution yielded good agreement with the experimental and numerical results; except for the cases of resonance, it suggested an unrealistic constant increase in pressures. The ALE numerical models reasonably captured the full time-series of all facets of water dynamic response, including pressures and wave heights for all cases.

It was demonstrated in this study that ALE numerical modeling is suitable for use in a performance-based design approach of complex fluid-structure-soil interaction problems. The ALE simulation, utilizing a single thread, displayed a runtime ranging from 2.5 to 10 min per second of motion (depending on the tank length), making it a viable approach for practical implementation in design processes. Therefore, it is recommended to employ analytical and simplified methods to obtain preliminary estimates only while utilizing ALE numerical modeling for final design. An extended experimental and numerical study that incorporates the full engineering system, featuring the components of structure, soil, and water, would be an important future work that will be carried out to further investigate the fluid-structure-soil interaction of water retaining structures such as buried water reservoirs.

ACKNOWLEDGMENTS

The authors gratefully acknowledge the funding provided by the National Science Foundation (NSF) under awards CMMI-1762749 and CMMI-1763129. The centrifuge facility at UC Davis is part of the NSF Natural Hazards Research Infrastructure

(NHERI) program under award CMMI-2037883. Any opinions, findings, conclusions, or recommendations expressed in this paper are solely those of the authors and do not necessarily reflect the views of the National Science Foundation. The authors thank Prof. Yasuo Sawamura, an Associate Professor at Kyoto University, for leading the first steps of designing the experiment. The authors thank the UC Davis Center for Geotechnical Modeling Associate Director Dan Wilson and staff (Tom Kohnke, Anatoliy Ganchenko, and Chad Justice) for making the experiments presented in this paper possible.

DATA AVAILABILITY STATEMENT

All experimental data are curated in DesignSafe and soon to be released. Some or all numerical models or codes that support the findings of this study are available upon reasonable request to the corresponding author.

ORCID

Karim AlKhatib https://orcid.org/0000-0002-7201-6752
Youssef M. A. Hashash https://orcid.org/0000-0002-0756-9027
Katerina Ziotopoulou https://orcid.org/0000-0001-5494-497X

REFERENCES

1. Ibrahim RA, Pilipchuk VN, Ikeda T. Recent advances in liquid sloshing dynamics. *Appl Mech Rev*. 2001;54:133-199. doi:10.1115/1.3097293
2. Cleary WA. Subdivision, stability, liability. *Mar Technol SNAME N*. 1982;19:228-244. doi:10.5957/mt1.1982.19.3.228
3. Bass R, Bowles E, Cox P. Liquid dynamic loads in LNG cargo tanks. *Soc Nav Architects Mar Eng Trans*. 1980;6:103-126.
4. Graham EW, Rodriguez AM. The characteristics of fuel motion which affect airplane dynamics. *J Appl Mech*. 1952;19:381-388.
5. Dodge FT. *The New Dynamic Behavior of Liquids in Moving Containers*. Southwest Research Inst; 2000.
6. Abramson HN. The dynamic behavior of liquids in moving containers, with applications to space vehicle technology. 1966; No. NASA-SP-106.
7. Housner GW. The dynamic behavior of water tanks. *Bull Seismol Soc Am*. 1963;53:381-387.
8. Westergaard HM. Water pressures on dams during earthquakes. *Trans ASCE*. 1933;98:418-433. doi:10.1061/TACEAT.0004496
9. EC8. *Eurocode 8 - Design of structures for earthquake resistance—Part 4: Silos, tanks and pipelines*. 2006.
10. *AWWA D110-13. Wire- and Strand-wound, Circular, Prestressed Concrete Water Tanks*. American Water Works Association. 2013.
11. *ACI 350.3-20. Code Requirements for Seismic Analysis and Design of Liquid-Containing Concrete Structures (ACI 350.3-20) and Commentary*. American Concrete Institute; 2021.
12. Chen Y, Xue MA. Numerical simulation of liquid sloshing with different filling levels using OpenFOAM and experimental validation. *Water*. 2018;10:1752.
13. Cruchaga MA, Reinoso RS, Storti MA, Celentano DJ, Tezduyar TE. Finite element computation and experimental validation of sloshing in rectangular tanks. *Comput Mech*. 2013;52:1301-1312.
14. Faltinsen OM, Rognebakke OF, Lukovsky IA, Timokha AN. Multidimensional modal analysis of nonlinear sloshing in a rectangular tank with finite water depth. *J Fluid Mech*. 2000;407:201-234. https://doi.org/10.1017/S0022112099007569
15. Goudarzi MA, Sabbagh-Yazdi SR. Investigation of nonlinear sloshing effects in seismically excited tanks. *Soil Dyn Earthq Eng*. 2012;43:355-365.
16. Battaglia L, Cruchaga M, Storti M, D'Elía J, Aedo JN, Reinoso R. Numerical modelling of 3D sloshing experiments in rectangular tanks. *Appl Math Model*. 2018;59:357-378.
17. Liu D, Lin P. A numerical study of three-dimensional liquid sloshing in tanks. *J Comput Phys*. 2008;227:3921-3939. doi:10.1016/j.jcp.2007.12.006
18. Song YK, Chang K-A, Ryu Y, Kwon SH. Experimental study on flow kinematics and impact pressure in liquid sloshing. *Exp Fluids*. 2013;54:1592.
19. Frandsen JB. Sloshing motions in excited tanks. *J Comput Phys*. 2004;196:53-87. doi:10.1016/j.jcp.2003.10.031
20. Gomez-Gesteira M, Rogers BD, Dalrymple RA, Crespo AJC. State-of-the-art of classical SPH for free-surface flows. *J Hydraul Res*. 2010;48:6-27.
21. Kozak AL, Tehrani PK, Abrahamson TE, Krimotat AV. Validation of the ALE Methodology by Comparison with the Experimental Data Obtained from a Sloshing Tank. In: 14th Int LS-DYNA Users Conference, 2016; Detroit, MI.
22. Yu CC, Whittaker AS. Verification of numerical models for seismic fluid-structure interaction analysis of internal components in liquid-filled advanced reactors. *Earthq Eng Struct Dyn*. 2021;50:1692-1712.
23. LSTC. LS-Dyna keyword user's manual. Livermore Software Technology Corporation. 2020.
24. *AWWA D100-21. Welded carbon steel tanks for water storage*. American Water Works Association; 2021.
25. Hunt B, Priestley N. Seismic water waves in a storage tank. *Bull Seismol Soc Am*. 1978;68:487-499. doi:10.1785/BSSA0680020487
26. Wu G, Ma Q, Taylor RE. Numerical simulation of sloshing waves in a 3D tank based on a finite element method. *Appl Ocean Res*. 1998;20:337-355.
27. Faltinsen OM. A numerical nonlinear method of sloshing in tanks with two-dimensional flow. *J Ship Res*. 1978;22:193-202.

28. Kotsubo S. Dynamic water pressure on dams during earthquakes. *In: Second world conference on earthquake engineering*. 1960:799-814.
29. Bustamante J, Rosenblueth E, Herrera I, Flores A. Presion hidrodinamica en presas y depositos. *Boletin Sociedad Mexicana de Ingenieria Sismica 1*. 1963.
30. Werner PW, Sundquist K. On hydrodynamic earthquake effects. *Eos Trans AGU*. 1949;30:636-657. doi:10.1029/TR030i005p00636
31. Epstein HI. Seismic design of liquid-storage tanks. *J Struct Div-ASCE*. 1976;102:1659-1673. doi:10.1061/JSDEAG.0004421
32. Kaminski ML, Bogaert H. Full-scale sloshing impact tests-Part I. *Int J Offshore Polar*. 2010;20.
33. Warnock JE. Hydraulic Similitude. In: Rouse H, ed. *Engineering Hydraulics*. John Wiley & Sons; 1950;136-176.
34. Garnier J, Gaudin C, Springman SM, et al. Catalogue of scaling laws and similitude questions in geotechnical centrifuge modelling. *Int J Phys Model Geo*. 2007;7:01-23.
35. Hughes SA. *Physical Models and Laboratory Techniques in Coastal Engineering*. World Scientific; 1993.
36. Sawyer BD. *Cone Penetration Testing of Coarse-Grained Soils in the Centrifuge to Examine the Effects of Soil Gradation and Centrifuge Scaling*. University of California; 2020.
37. Morales B. *Centrifuge Modeling of Hydrodynamic Loads in Water Storage Tanks*. University of California; 2020
38. Gillis K, Dashti S, Hashash YMA. Dynamic calibration of tactile sensors for measurement of soil pressures in centrifuge. *Geotech Test J*. 2015;38:261-274.
39. Kutter B, Idriss I, Khonke T, et al. Design of a large earthquake simulator at UC Davis. In: Int Conf centrifuge. Rotterdam, The Netherlands; 1994; 169–175.
40. Mason HB, Kutter BL, Bray JD, Wilson DW, Choy BY. Earthquake motion selection and calibration for use in a geotechnical centrifuge. In: 7th International Conference on Physical Modeling in Geotechnics; 2010; 361–366.
41. Doğangün A, Durmuş A, Ayvaz Y. Static and dynamic analysis of rectangular tanks by using the Lagrangian fluid finite element. *Comput Struct*. 1996;59:547-552.
42. Donea J, Huerta A, Ponthot J-P, Rodríguez-Ferran A. Arbitrary Lagrangian–Eulerian methods. In: Stein E, Borst R, Hughes TJR, eds. *The Encyclopedia of Computational Mechanics*. Wiley. 2004;413-437.
43. Monaghan JJ. Smoothed particle hydrodynamics. *Annu Rev Astron Astrophys*. 1992;30:543-574.
44. Hertel ES. The CTH data interface for equation-of-state and constitutive model parameters. *Sandia Report*. 1992. SAND92-1297.
45. Lambe T. Predictions in soil engineering. *Géotechnique*. 1973;23:151-202.

How to cite this article: AlKhatib K, Hashash YMA, Ziotopoulou K, Morales B. Hydrodynamic pressures on rigid walls subjected to cyclic and seismic ground motions. *Earthquake Engng Struct Dyn*. 2023;1-24. https://doi.org/10.1002/eqe.4020